Infrared Action Spectra of $Ca^{2+}(H_2O)_{11-69}$ Exhibit Spectral Signatures for Condensed-Phase Structures with Increasing Cluster Size

Matthew F. Bush, Richard J. Saykally, and Evan R. Williams*

Department of Chemistry, University of California, Berkeley, California 94720-1460

Received June 17, 2008; E-mail: williams@cchem.berkeley.edu

Abstract: Infrared laser action spectroscopy is used to characterize divalent calcium ions solvated by up to 69 water molecules. The spectrum for $Ca^{2+}(H_2O)_{12}$ indicates that in the predominant structure, eight inner-shell water molecules solvate the metal ion and donate one hydrogen bond to one of four second-shell, double-acceptor water molecules. Eight-coordinate solvation is consistent with results from many condensed-phase studies, and contrasts with results for smaller gas-phase clusters that are most consistent with six-coordinate solvation. Each water molecule in this structure of $Ca^{2+}(H_2O)_{12}$ coordinates with two other members of the cluster. With increasing cluster size, the number of two-coordinate water molecules decreases, whereas that of three-coordinate water molecules increases. The number of one-coordinate water molecules increases until $n \approx 18$, but they are essentially depleted by $n \approx 30$. Spectra of the largest clusters, which have effective concentrations of divalent calcium that are less than 1 M, exhibit only subtle changes with increasing cluster size. The bonded-OH regions of these spectra are similar to, but blue-shifted from that of bulk water, whereas the free-OH regions are well-resolved and indicate that the surfaces of these clusters are well-structured. These results comprise the most extensive vibrational spectroscopic study yet performed on metal ion hydration in the gas phase and provide insights into metal ion solvation in bulk and interfacial environments.

Introduction

Water structure in the presence of ions reflects a delicate balance between ion–water interactions and intrinsic solvent hydrogen bonding. Studies of small hydrated ion clusters can reveal detailed information about direct ion/solvent interactions. For example, sequential water binding energies measured by a variety of techniques reveal the thermochemistry of the initial ion solvation process[1–3] and infrared action spectra provide associated structural information.[4–15] Ions also affect solvent properties through indirect interactions with the hydrogen-bond network. Results from studies of increasingly large clusters can be extrapolated to reveal information about the structures and reactivities of ions in solution and near interfaces, including phenomena that have not been measured directly in condensed-phase experiments. For example, photoelectron spectra of sequentially larger hydrated electron clusters have been studied to determine thermodynamic values for electrons in bulk-water environments,[16] electron recombination energies for solvated metal ion clusters have been used to obtain absolute electrochemical potentials in solution,[17] and infrared multiple photon dissociation (IRMPD) action spectra of $H^+(H_2O)_{21}$ have been used as evidence to support structures in which the excess charge is localized at the cluster surface,[18–21] which is consistent with

(1) Peschke, M.; Blades, A. T.; Kebarle, P. *J. Phys. Chem. A* **1998**, *102*, 9978–9985.
(2) Rodriguez-Cruz, S. E.; Jockusch, R. A.; Williams, E. R. *J. Am. Chem. Soc.* **1999**, *121*, 8898–8906.
(3) Carl, D. R.; Moision, R. M.; Armentrout, P. B. *Int. J. Mass Spectrom.* **2007**, *265*, 308–325.
(4) Miller, D. J.; Lisy, J. M. *J. Chem. Phys.* **2006**, *124*, 024319.
(5) Robertson, W. H.; Johnson, M. A. *Annu. Rev. Phys. Chem.* **2003**, *54*, 173–213.
(6) Inokuchi, Y.; Ohshimo, K.; Misaizu, F.; Nishi, N. *J. Phys. Chem. A* **2004**, *108*, 5034–5040.
(7) Walters, R. S.; Pillai, E. D.; Duncan, M. A. *J. Am. Chem. Soc.* **2005**, *127*, 16599–16610.
(8) Bush, M. F.; Saykally, R. J.; Williams, E. R. *ChemPhysChem* **2007**, *8*, 2245–2253.
(9) Bush, M. F.; Saykally, R. J.; Williams, E. R. *J. Am. Chem. Soc.* **2008**, *130*, 9122–9128.
(10) O'Brien, J. T.; Williams, E. R. *J. Phys. Chem. A* **2008**, *112*, 5893–5901.
(11) Kamariotis, A.; Boyarkin, O. V.; Mercier, S.; Beck, R. D.; Bush, M. F.; Williams, E. R.; Rizzo, T. R. *J. Am. Chem. Soc.* **2006**, *128*, 905–916.
(12) Bush, M. F.; Saykally, R. J.; Williams, E. R. *J. Am. Chem. Soc.* **2007**, *129*, 2220–2221.
(13) Zhou, J.; Santambrogio, G.; Brümmer, M.; Moore, D. T.; Wöste, L.; Meijer, G.; Neumark, D. M.; Asmis, K. R. *J. Chem. Phys.* **2006**, *125*, 111102.
(14) Yeh, L. I.; Okumura, M.; Myers, J. D.; Price, J. M.; Lee, Y. T. *J. Chem. Phys.* **1989**, *91*, 7319–7330.
(15) Carnegie, P. D.; Bandyopadhyay, B.; Duncan, M. A. *J. Phys. Chem. A* **2008**, *112*, 6237–6243.
(16) Coe, J. V.; Williams, S. M.; Bowen, K. H. *Int. Rev. Phys. Chem.* **2008**, *27*, 27–51.
(17) Donald, W. A.; Leib, R. D.; O'Brien, J. T.; Bush, M. F.; Williams, E. R. *J. Am. Chem. Soc.* **2008**, *130*, 3371–3381.
(18) Shin, J. W.; Hammer, N. I.; Diken, E. G.; Johnson, M. A.; Walters, R. S.; Jaeger, T. D.; Duncan, M. A.; Christie, R. A.; Jordan, K. D. *Science* **2004**, *304*, 1137–1140.
(19) Miyazaki, M.; Fujii, A.; Ebata, T.; Mikami, N. *Science* **2004**, *304*, 1134–1137.
(20) Chang, H. C.; Wu, C. C.; Kuo, J. L. *Int. Rev. Phys. Chem.* **2005**, *24*, 553–578.
(21) Iyengar, S. S. *J. Chem. Phys.* **2007**, *126*, 216101.

condensed-phase experiments that indicate enhanced concentrations of hydrated protons at the air/water interface.[22,23]

IRMPD action spectroscopy has yielded valuable insights into the structures of many singly charged hydrated ions, including e^-,[24] Cl^-,[5,25] H^+,[14,18−20,26,27] K^+,[4] Mg^{+},[6] and Ni^{+},[7] and has recently been demonstrated for multiply charged hydrated cations[8−10] and anions.[12,13] IRMPD spectra of $Ca^{2+}(H_2O)_{4−10}$ indicate that the first six water molecules coordinate directly with the metal ion and additional water molecules occupy positions in outer solvent shells.[8] The coordination number (CN), or the number of water molecules directly coordinated to the metal ion, is six for these clusters. This value is consistent with many results for small clusters, including binding energies measured by high pressure mass spectrometry,[1] blackbody infrared radiative dissociation,[2] and guided ion beam mass spectrometry[3] experiments, as well as calculations at the density functional[2,3,8,28] and MP2 levels of theory.[3] Solvation of aqueous divalent calcium has been investigated by a variety of methods, including X-ray diffraction,[29−32] X-ray absorption spectroscopy,[29,33] neutron diffraction,[34,35] classical molecular dynamics (MD),[29,36−39] hybrid quantum mechanical/molecular mechanics MD,[38−40] and Carr−Parrinello MD.[41−44] Most studies provide support for solution-phase CN values ranging from seven to eight,[29−33,35−42,44] although the full range of reported CN values, inclusive of uncertainties, extends from $5 - 10$.[30,32−34,39,41−43] Differences between gas- and condensed-phase water CN values have been previously noted for other cations. The CN of trivalent

rare earth metal ions in aqueous solution range from 8 to 9, but the IRMPD spectra of $M^{3+}(H_2O)_{20}$, M = Y, La, Pr, Tb, and Tm, exhibit no discernible dependence on metal ion identity, which suggests similar hydration structures.[9] Divalent copper is thought to have a CN = 6 in aqueous solution, but results from IRMPD spectroscopy[10] and *ab initio* calculations[10,45,46] indicate a CN = 4 for $Cu^{2+}(H_2O)_6$ and the presence of a third solvent shell for $n \geq 10$.[10] The CN of K^+ in small gas-phase clusters with para-difluorobenzene has been shown to be similar to that of K^+ in aqueous solution and greater than that in small gas-phase clusters with water.[4]

Here, a multiplexed experimental protocol is used to obtain infrared photodissociation spectra of selected $Ca^{2+}(H_2O)_{11−69}$ clusters. Comparisons between the IRMPD spectra and with calculated spectra for candidate structures indicate that the CN for these larger clusters is greater than that observed for smaller clusters and similar to that observed in solution. Additionally, the spectra of the largest clusters exhibit only subtle changes with increasing cluster size, suggesting that intrinsic water properties are increasingly predominant with increasing cluster size.

Methods

Experimental Methods. Experiments were performed on a 2.7 T Fourier-transform ion cyclotron resonance mass spectrometer.[8,47] $Ca^{2+}(H_2O)_n$ clusters are formed by nanoelectrospray ionization from 1 mM aqueous solutions of $CaCl_2$ using a home-built electrospray interface. Ion abundances for the clusters of interest were optimized by adjusting interface and trapping conditions.[9,48] Ions were trapped in a cylindrical ion cell that is surrounded by a copper jacket; the temperature of the jacket is regulated by either a controlled liquid nitrogen flow[49] or by continuous contact with liquid nitrogen supplied by a custom-built, gravity fed dewar. The clusters of interest were isolated using a stored waveform inverse Fourier transform pulse and subsequently irradiated with 7−30 pulses of IR radiation (8−21 mJ per ~6 ns pulse) from a tunable 10 Hz optical parametric oscillator/amplifier (LaserVision, Bellevue, WA). IRMPD spectra were obtained by plotting the power- and time-corrected photodissociation intensity as a function of laser frequency.[47]

Computational Methods. The enormous conformational space of large clusters presents a challenge in both identifying low-energy structures and calculating thermochemical values accurately.[50] A limited number of candidate low-energy structures were determined using conformational searching and chemical intuition. Initial structures were generated using Monte Carlo conformation searching with the MMFFs force field as implemented in Macromodel 8.1 (Schrödinger, Inc. Portland, OR) and by adding or removing water molecules from low-energy structures. Candidate structures were energy minimized and vibrational frequencies were calculated using the harmonic oscillator approximation using hybrid method density functional calculations (B3LYP) and the 6−311++G(d,p) basis set as implemented in Gaussian 03.[51] Vibrational frequencies were scaled by 0.963, which provides good agreement with

(22) Petersen, P. B.; Saykally, R. J. *J. Phys. Chem. B* **2005**, *109*, 7976–7980.
(23) Levering, L. M.; Sierra-Hernandez, M. R.; Allen, H. C. *J. Phys. Chem. C* **2007**, *111*, 8814–8826.
(24) Asmis, K. R.; Santambrogio, G.; Zhou, J.; Garand, E.; Headrick, J.; Goebbert, D.; Johnson, M. A.; Neumark, D. M. *J. Chem. Phys.* **2007**, *126*, 191105.
(25) Choi, J. H.; Kuwata, K. T.; Cao, Y. B.; Okumura, M. *J. Phys. Chem. A* **1998**, *102*, 503–507.
(26) Jiang, J. C.; Wang, Y. S.; Chang, H. C.; Lin, S. H.; Lee, Y. T.; Niedner-Schatteburg, G. *J. Am. Chem. Soc.* **2000**, *122*, 1398–1410.
(27) Wu, C. C.; Lin, C. K.; Chang, H. C.; Jiang, J. C.; Kuo, J. L.; Klein, M. L. *J. Chem. Phys.* **2005**, *122*, 074315.
(28) Pavlov, M.; Siegbahn, P. E. M.; Sandström, M. *J. Phys. Chem. A* **1998**, *102*, 219–228.
(29) Jalilehvand, F.; Spångberg, D.; Lindqvist-Reis, P.; Hermansson, K.; Persson, I.; Sandström, M. *J. Am. Chem. Soc.* **2001**, *123*, 431–441.
(30) Probst, M. M.; Radnai, T.; Heinzinger, K.; Bopp, P.; Rode, B. M. *J. Phys. Chem.* **1985**, *89*, 753–759.
(31) Smirnov, P.; Yamagami, M.; Wakita, H.; Yamaguchi, T. *J. Mol. Liq.* **1997**, *73–74*, 305–316.
(32) Megyes, T.; Grósz, T.; Radnai, T.; Bakó, I.; Pálinkás, G. *J. Phys. Chem. A* **2004**, *108*, 7261–7271.
(33) Fulton, J. L.; Heald, S. M.; Badyal, Y. S.; Simonson, J. M. *J. Phys. Chem. A* **2003**, *107*, 4688–4696.
(34) Hewish, N. A.; Neilson, G. W.; Enderby, J. E. *Nature* **1982**, *297*, 138–139.
(35) Badyal, Y. S.; Barnes, A. C.; Cuello, G. J.; Simonson, J. M. *J. Phys. Chem. A* **2004**, *108*, 11819–11827.
(36) Jiao, D.; King, C.; Grossfield, A.; Darden, T. A.; Ren, P. Y. *J. Phys. Chem. B* **2006**, *110*, 18553–18559.
(37) Obst, S.; Bradaczek, H. *J. Phys. Chem.* **1996**, *100*, 15677–15687.
(38) Schwenk, C. F.; Loeffler, H. H.; Rode, B. M. *J. Chem. Phys.* **2001**, *115*, 10808–10813.
(39) Tongraar, A.; Liedl, K. R.; Rode, B. M. *J. Phys. Chem. A* **1997**, *101*, 6299–6309.
(40) Tofteberg, T.; Ohrn, A.; Karlstrom, G. *Chem. Phys. Lett.* **2006**, *429*, 436–439.
(41) Lightstone, F. C.; Schwegler, E.; Allesch, M.; Gygi, F.; Galli, G. *ChemPhysChem* **2005**, *6*, 1745–1749.
(42) Ikeda, T.; Boero, M.; Terakura, K. *J. Chem. Phys.* **2007**, *127*, 074503.
(43) Bako, I.; Hutter, J.; Palinkas, G. *J. Chem. Phys.* **2002**, *117*, 9838–9843.
(44) Naor, M. M.; Van Nostrand, K.; Dellago, C. *Chem. Phys. Lett.* **2003**, *369*, 159–164.

(45) Bérces, A.; Nukada, T.; Margl, P.; Ziegler, T. *J. Phys. Chem. A* **1999**, *103*, 9693–9701.
(46) Bryantsev, V. S.; Diallo, M. S.; van Duin, A. C. T.; Goddard, W. A., III. *J. Phys. Chem. A* **2008**, *112*, 9104–9112.
(47) Bush, M. F.; O'Brien, J. T.; Prell, J. S.; Saykally, R. J.; Williams, E. R. *J. Am. Chem. Soc.* **2007**, *129*, 1612–1622.
(48) Bush, M. F.; Saykally, R. J.; Williams, E. R. *Int. J. Mass Spectrom.* **2006**, *253*, 256–262.
(49) Wong, R. L.; Paech, K.; Williams, E. R. *Int. J. Mass Spectrom.* **2004**, *232*, 59–66.
(50) Rotzinger, F. P. *J. Phys. Chem. B* **2005**, *109*, 1510–1527.
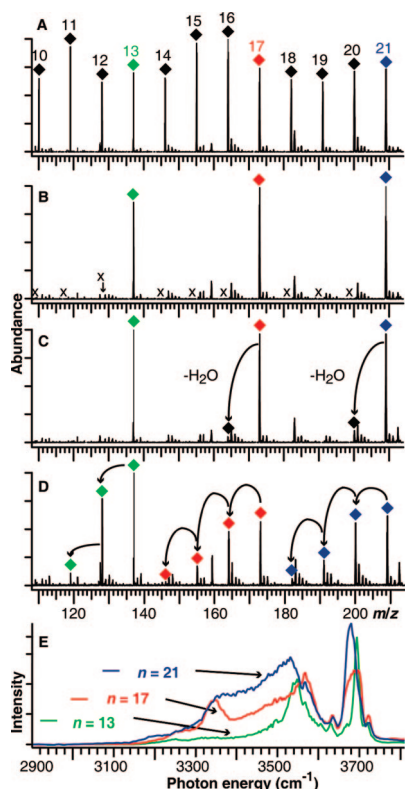(51) Frisch, M. J.; et al. *Gaussian03*, revision B.04; Gaussian, Inc.: Wallingford, CT, 2004.

Figure 1. Sample data illustrating the simultaneous acquisition of photodissociation spectra of $Ca^{2+}(H_2O)_{13,17,21}$. $Ca^{2+}(H_2O)_n$ formed by electrospray are accumulated (A) and the monoisotopic clusters of interest are isolated from the distribution (B). A 1.0 s BIRD mass spectrum shows the dissociation in the absence of laser irradiation (C). Mass spectra are acquired after laser irradiation (D, 1.0 s at 3555 cm^{-1}) as function of frequency. After background subtraction, this process yields multiple infrared spectra with directly comparable intensities (E).

photodissociation spectra in the free-OH stretch region. This scaling factor is greater than that used in our previous investigation of $Ca^{2+}(H_2O)_n$ (0.95), but a smaller basis set was used in that study.[8] In order to approximate some of the temperature effects in the photodissociation spectra, line spectra were convolved using 10 cm^{-1} fwhm Lorentzian distributions for the nonbonded stretches and 50 cm^{-1} for the bonded stretches.

Results and Discussion

Photodissociation and Multiplexed Data Acquisition. The distribution of $Ca^{2+}(H_2O)_n$ formed by nanoelectrospray ionization is generally broad and can be shifted to larger or smaller sizes by changing experimental parameters, such as the temperature of the heated metal capillary.[48] A mass spectrum obtained under conditions optimized for $n \approx 16$ is shown in Figure 1A. Multiple precursor ions are isolated from this distribution (Figure 1B) using a stored waveform inverse Fourier transform (SWIFT) pulse. Figure 1C shows the blackbody infrared radiative dissociation (BIRD) that occurs in the absence of laser irradiation.[2,49] Irradiation by resonant light generated by a tunable optical parametric oscillator/amplifier results in the sequential loss of one or more water molecules (Figure 1D). Because multiple laser pulses are used, product ions are also exposed to laser photons and may subsequently photodissociate. Careful choice of precursor sizes and laser irradiation times are required to ensure that product ions formed by sequential loss of water molecules from a larger cluster do not interfere with a smaller isolated precursor. This method is similar to that used

by Oomens et al. to simultaneously measure the IRMPD spectra of multiple charge states of cyctochrome c.[52]

The photodissociation rate is determined from the relative abundances of the precursor and product ions, and the irradiation time using eq 1:

$$k_{photodissociation} = \ln\left\{\frac{[Precursor\ Ion]}{[Precursor\ Ion] + \sum[Product\ Ion]}\right\}\Big/time$$

(1)

The photodissociation rate is corrected for background BIRD and the frequency dependent laser power using eq 2:

$$Intensity = \frac{k_{photodissociation} - k_{BIRD}}{power(\nu)}$$

(2)

This yields a photodissociation intensity that has units of $s^{-1}W^{-1}$ and accounts for sequential dissociation of product ions, irradiation time, background BIRD, and the frequency dependent laser power.[8,47] Repeating this process as a function of laser frequency yields multiple infrared action spectra that are acquired simultaneously (Figure 1E).

This method for spectral acquisition has the advantage that the spectra of multiple precursor ions are measured simultaneously, which significantly increases the efficiency of data acquisition. In these experiments, 2 or 3 photodissociation spectra were typically acquired in parallel, but in principle, many more could be acquired at the same time. Simultaneously measuring precursor and product ion abundances eliminates effects of variations in precursor ion intensity caused by fluctuations in the ESI source. Equally significant is the fact that simultaneously trapped precursor ions are exposed to identical fluxes of blackbody and laser radiation, making it possible to directly compare relative intensities in the simultaneously acquired photodissociation spectra (Figure 1E).

One potential complication in the interpretation of action spectroscopy experiments is that photodissociation intensities may differ from those obtained from linear absorption spectroscopy and calculated infrared spectra. However, such effects are expected to be small in these experiments because photon energies should be comparable to the water binding energies of these ions.[1,49,53] The mass spectra exhibit no particularly intense peaks, suggesting the absence of any significant "magic number" effects, and differences in water binding energies over this size range should be small.[1,49,53] Additionally, ions under these conditions possess considerable internal energy prior to laser irradiation, which is evident from the observation of BIRD from all but the smallest ions. Because the absorption of just one laser photon should increase the photodissociation rate in these experiments, relative intensities between simultaneously acquired action spectra are expected to be similar to those of true absorption spectra. However, the sequential absorption of multiple photons almost certainly occurs. Therefore, the experimental spectra are referred to as infrared multiple photon dissociation (IRMPD) spectra to reflect contributions from sequential absorption of multiple photons and to emphasize the potential differences between these action spectra and linear absorption spectra. The role of single versus multiple photon absorption as a function of cluster size, laser fluence, and copper

(52) Oomens, J.; Polfer, N.; Moore, D. T.; van der Meer, L.; Marshall, A. G.; Eyler, J. R.; Meijer, G.; von Helden, G. *Phys. Chem. Chem. Phys.* **2005**, *7*, 1345–1348.
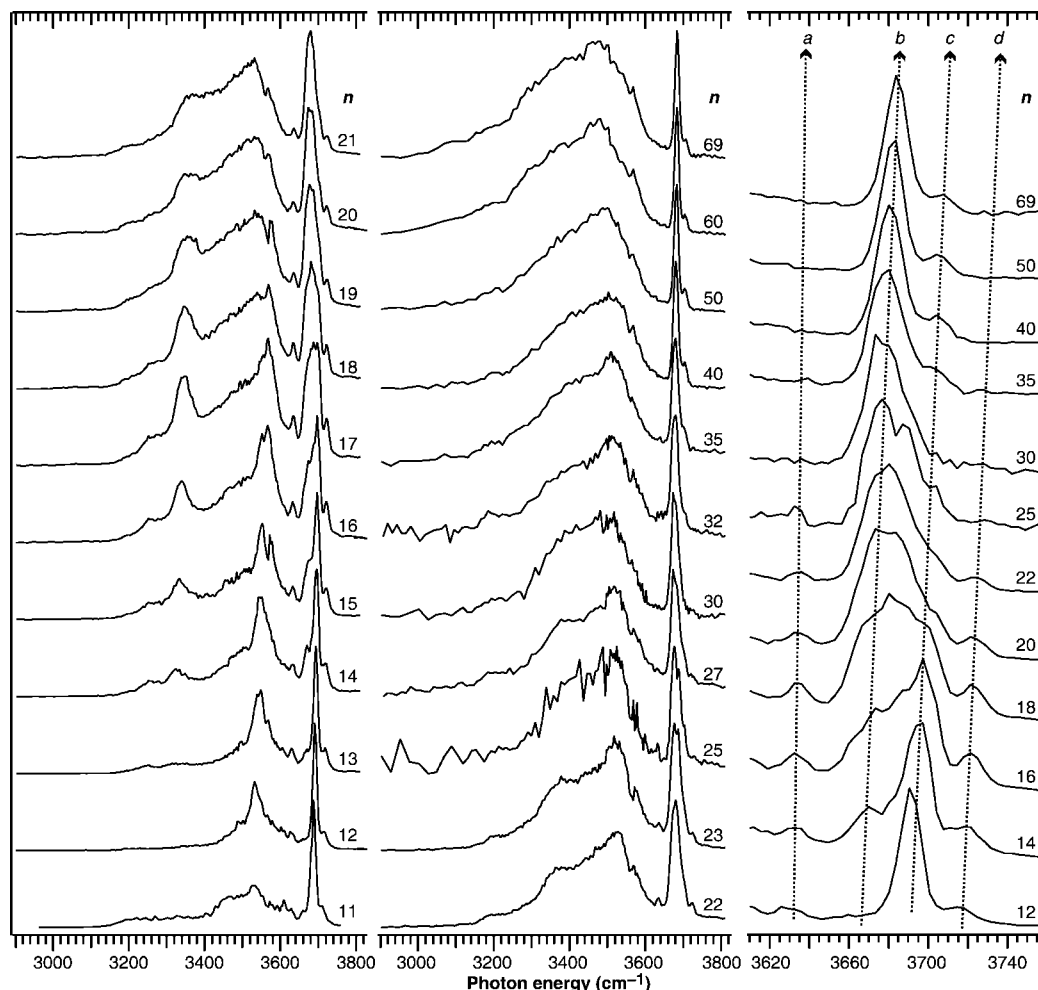(53) Donald, W. A.; Williams, E. R. *J. Phys. Chem. A* **2008**, *112*, 3515–3522.

Figure 2. Photodissociation spectra of Ca^{2+}(H$_2$O)$_n$ obtained with a copper jacket temperature of 130 K (150 K for $n = 11$).

jacket temperature can be elucidated by modeling the radiative absorption, radiative emission, and dissociation using a master equation approach.[54] This process would also yield the effective temperatures of ions in these experiments.

Infrared Action Spectra. Using this multiplexed data acquisition method, infrared action spectra were measured for selected Ca^{2+}(H$_2$O)$_n$, $n = 11-69$ (Figure 2). These spectra exhibit many bands that persist and evolve with increasing n. Many of these bands and trends are similar to those observed for other hydrated ions, particularly H$^+$(H$_2$O)$_n$[18,20] and Ca^{2+}(H$_2$O)$_n$, $n = 4-10$.[8] A few key results from those studies are discussed below and will be used extensively to interpret the spectra of Ca^{2+}(H$_2$O)$_n$, $n = 11-69$.

The high-frequency region of these spectra is where the stretching modes occur for hydroxyl groups that do not donate a hydrogen bond (free-OH) and these bands are especially useful for characterizing hydrated ion structure.[7,8,11,18–20,55] These modes exhibit four bands in this region,[56] denoted $a-d$ using the notation of Shin et al.,[18] that are qualitatively similar to those observed for many hydrated ions, including H$^+$(H$_2$O)$_n$.[18,20,26] These bands for H$^+$(H$_2$O)$_n$ have been assigned to the free-OH

(54) Price, W. D.; Schnier, P. D.; Jockusch, R. A.; Strittmatter, E. F.; Williams, E. R. *J. Am. Chem. Soc.* **1996**, *118*, 10640–10644.

(55) Bush, M. F.; Prell, J. S.; Saykally, R. J.; Williams, E. R. *J. Am. Chem. Soc.* **2007**, *129*, 13544–13553.

(56) Bands *b* and *c* are poorly resolved for all except the very largest ions, but are clearly present for all except the very smallest ions.
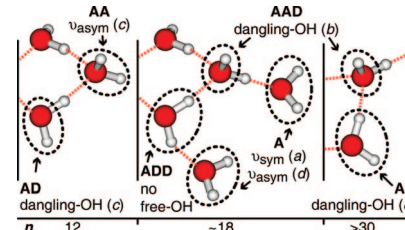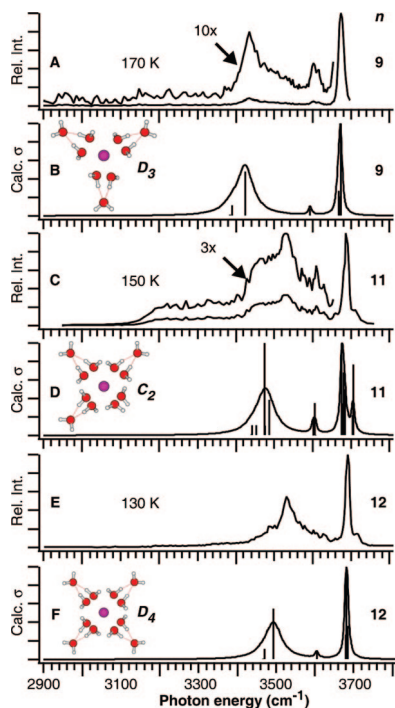

Figure 3. Acceptor (**A**) and donor (**D**) hydrogen bonding configurations expected to contribute bands (noted in lower-case italics and marked in Figure 2) to the free-OH regions of the IRMPD spectra. The *n* values correspond to sizes for which these configurations are predominant.

stretches of water molecules in different hydrogen bonding configurations,[18,20,26] which are shown schematically in Figure 3. The term acceptor refers to water molecules that either accept a hydrogen bond from another water molecule or interact directly with the metal ion. The term donor refers to water molecules that donate a hydrogen bond to another water molecule. Bands *a* and *d* are assigned to the symmetric and asymmetric stretches of single-acceptor only water molecules (**A**, one-coordinate water), respectively. Band *b* is assigned to the dangling-OH stretches of double-acceptor–single-donor water molecules (**AAD**, three-coordinate water).[18,20] Band *c* is assigned to both the dangling-OH stretches of single-acceptor–single-donor (**AD**) water molecules[18,20] and the asym-

Figure 4. Photodissociation spectra of $Ca^{2+}(H_2O)_n$, $n = 9$ (A),[8] 11 (C), and 12 (E). Copper jacket temperatures are noted on individual spectra. B3LYP/6−311++G(d,p) calculated spectra for these ions are shown in B, D, and F, respectively.

metric stretch of **AA** water molecules,[8] which are both two-coordinate motifs.

The low-frequency region of these spectra is where the stretching modes occur for hydroxyl groups that do donate a hydrogen bond (bonded-OH). As discussed by Duncan and co-workers,[7] the most red-shifted bands in the bonded-OH region are attributable to hydroxyl groups that donate a hydrogen bond to outer-shell, single-acceptor only water molecules, whereas the less red-shifted bands in the bonded-OH region are attributable to water molecules that accept and donate additional hydrogen bonds and are involved in hydrogen-bonding networks. However, assigning photodissociation spectra in this region to specific hydrogen bonding motifs is more challenging with increasing cluster size because of spectral congestion[18] and finite temperature effects.[21]

Effect of Cluster Size on Coordination Number. The IRMPD spectrum of $Ca^{2+}(H_2O)_{11}$ exhibits many bands that that are similar to those observed previously for $Ca^{2+}(H_2O)_9$. The IRMPD spectrum of $Ca^{2+}(H_2O)_9$ (Figure 4A) is most consistent with a structure in which six inner-shell, **AD** water molecules each donate a single hydrogen bond to one of three second-shell, **AA** water molecules (D_3 symmetry, Figure 4B).[8] The calculated spectrum has relatively few bands; the asymmetric stretches of the **AA** water molecules and the nonbonded hydrogen stretches (dangling-OH) stretches of the **AD** water molecules are superimposed and yield a single band near 3670 cm^{-1} (band c), the symmetric stretches of the **AA** water molecules are calculated to occur at 3593 cm^{-1} (band a), and the in-phase and out-of-phase bonded hydrogen stretches are calculated to occur at 3390 and 3424 cm^{-1}, respectively. Additional candidate structures and the weak photodissociation intensities observed in the bonded-OH region have been discussed previously for $Ca^{2+}(H_2O)_9$.[8]

The IRMPD spectrum of $Ca^{2+}(H_2O)_{11}$ also exhibits broad photodissociation from 3100 − 3400 cm^{-1} and additional bands

at 3530 and 3660 cm^{-1} (Figure 4C). These additional features were also observed at weaker intensities for $Ca^{2+}(H_2O)_{10}$ and indicate new hydrogen bonding configurations. Changes in ion structure are required because it is no longer possible to have an octahedral inner shell consisting of **AD** water molecules that donate only a single hydrogen bond to **AA** water molecules in the second solvent shell, like the predominant structure identified for $Ca^{2+}(H_2O)_9$. One possibility is that $Ca^{2+}(H_2O)_{10−11}$ clusters adopt structures with higher CN values. Figure 4D shows a structure of $Ca^{2+}(H_2O)_{11}$ with CN = 8 that has similar hydrogen bonding configurations to those identified for $Ca^{2+}(H_2O)_9$, but the calculated absorption spectrum of this structure does not account for the photodissociation intensity observed below 3400 cm^{-1} in the IRMPD spectrum.

The additional spectral features observed for $Ca^{2+}(H_2O)_{11}$ are instead most consistent with populations of structures containing water molecules that donate a hydrogen bond to a single-acceptor (**A**) water molecule, as discussed previously for $Ca^{2+}(H_2O)_{10}$.[8] For example, two of the low-energy structures identified for $Ca^{2+}(H_2O)_{10}$ have nine water molecules in positions very similar to that shown in Figure 4B for $Ca^{2+}(H_2O)_9$.[8] In one, the additional water molecule accepts a single hydrogen bond from an **AA** water molecule in the second shell of the $n = 9$ structure, yielding **A** and **AAD** water molecules in the $n = 10$ structure (previously labeled 10C).[8] The bonded-OH and dangling-OH stretches of the **AAD** water molecule are calculated to occur at 3108 and 3650 cm^{-1}.[8] In the other, the additional water molecule accepts a single hydrogen bond from an **AD** water molecule in the first shell of the $n = 9$ structure, yielding **A** and **ADD** water molecules in the $n = 10$ structure (previously labeled 10D).[8] The symmetric and asymmetric stretches of the **ADD** water molecule are calculated to occur at 3247 and 3512 cm^{-1}.[8] Both of these low-energy structures of $Ca^{2+}(H_2O)_{10}$ have **A** water molecules in outer solvent shells that are calculated to have symmetric and asymmetric stretches at 3611 − 3612 and 3707 − 3709 cm^{-1}, respectively. The new spectral features observed for $Ca^{2+}(H_2O)_{10−11}$ can be explained by populations of structures containing **A**, **AAD**, and **ADD** water molecules. There are almost certainly multiple structures, perhaps even additional hydrogen bonding motifs, contributing to each IRMPD spectrum.

The IRMPD spectrum of $Ca^{2+}(H_2O)_{12}$ is greatly simplified (Figure 4E). The bands below 3500 cm^{-1} are nearly absent and the remaining bands are similar to, but blue-shifted from those observed for $Ca^{2+}(H_2O)_9$. This precludes the new binding motifs identified for $Ca^{2+}(H_2O)_n$, $n = 10$ and 11, and suggests a structure with similar water coordination motifs to those identified for $Ca^{2+}(H_2O)_9$. This assignment is strongly supported through comparisons with the spectrum calculated for the structure in Figure 4F. By contrast, the photodissociation spectrum of $Ca^{2+}(H_2O)_{11}$ has many features that are not predicted for the structure formed by removing a second shell water molecule from the structure identified for $n = 12$ (Figure 4D), indicating that an important structural transition corresponding to an increased CN value of 8 occurs between clusters with 11 and 12 water molecules. This CN value is consistent with many results for divalent calcium in bulk aqueous solution.[29−31,33,35−42,44]

The most intense bonded-OH band for $Ca^{2+}(H_2O)_{12}$ (3530 cm^{-1}) is considerably blue-shifted from that observed for $Ca^{2+}(H_2O)_9$ (3435 cm^{-1}), which is consistent with increased CN and decreased charge transfer from any given water molecule to the metal ion in the larger cluster.[7,8] Interestingly,

these frequencies are both blue-shifted from those calculated for the assigned predominant structure (3493 cm^{-1} in Figure 4F, 3424 cm^{-1} in Figure 4B). Alternative hydrogen bonding configurations that are calculated to have frequencies that better match these experimental band frequencies, such as the asymmetric stretch of **ADD** water molecules, also have additional bands at lower frequencies that are incompatible with the IRMPD spectrum.[8] Therefore, these apparent discrepancies between experiment and theory are most likely attributable to the use of the harmonic oscillator approximation and a single scaling factor (0.963) for all calculated vibrational modes, even though different hydrogen bonding configurations almost certainly have different anharmonicities. Such differences illustrate the challenges in assigning individual action spectra through comparisons with individual calculated action spectra. It is likely that the most reliable assignments can be drawn through comparisons with action spectra of reference ions, *i.e.*, clusters that contain a different cation or different number of water molecules.

Band Evolution for $n = 13-18$. The relative intensities of bands *a* and *d*, which are spectral signatures for **A** water molecules, and band *b*, which is a spectral signature for **AAD** water molecules, both increase between $n = 13 - 18$, whereas that for band *c* decreases (Figure 2). The increasing relative intensities of bands *a*, *b*, and *d* relative to band *c* is most consistent with the presence of additional one- and three-coordinate water molecule binding motifs, relative to the two-coordinate binding motifs identified for $Ca^{2+}(H_2O)_{12}$. For example, if an **AD** water molecule forms a new hydrogen bond to a free water molecule, the former would adopt an **ADD** configuration and exhibit no free-OH bands (band *c* depleted), whereas the later would adopt an **A** configuration and exhibit bands *a* and *d* (Figure 3). Alternatively, if an **AA** water molecule forms a new hydrogen bond to a free water molecule, the former would adopt an **AAD** configuration and exhibit band *b* (band *c* depleted), whereas the later would adopt an **A** configuration and exhibit bands *a* and *d* (Figure 3).

The hydrogen-bonding motifs suggested by the new free-OH bands for $Ca^{2+}(H_2O)_n$ over this size range will also result in new bonded-OH bands. Based on calculations for $Ca^{2+}(H_2O)_{10}$ reported previously and discussed above, the new bands near 3340 and 3560 cm^{-1} are consistent with the symmetric and asymmetric stretches of double donor water molecules. The large frequency difference between these two bands can be attributed to the difference in hydrogen bonding strengths to the two acceptors.[8,57] The asymmetric stretches of **ADD** water molecules are observed near 3600 cm^{-1} for slightly larger $H^+(H_2O)_n$ and are well resolved from the other bonded-OH bands.[18] The new band near 3250 cm^{-1} is consistent with the bonded stretch of a hydroxyl group that donates a hydrogen bond to an **A** water molecule. It is also possible that the intensities in this region are affect by Fermi resonances with water bend overtones, which further complicates spectral interpretation.[58,59]

Band Evolution for $n > 18$. In the free-OH region, bands *a*, *c*, and *d* decrease in intensity relative to band *b* with increasing *n*. Bands *a* and *d* are nearly depleted by $n \approx 30$, whereas band
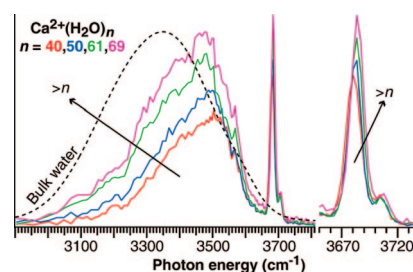

Figure 5. Photodissociation spectra of $Ca^{2+}(H_2O)_{40,50,61,69}$ obtained with a copper jacket temperature of 130 K. Bulk water spectrum is convoluted from parameters reported by Allen and co-workers.[23]

c persists in all spectra. This indicates that populations of one- and two-coordinate water molecules are depleted with increasing cluster size, and that populations of water molecules with higher coordination numbers are predominant. In the bonded-OH region, the relative photodissociation intensities from 3350 − 3500 cm^{-1} increase with *n* relative to the bonded-OH bands above and below this range that were most intense for smaller *n*. This new band occurs at frequencies similar to, but somewhat blue-shifted from the absorbance maximum of bulk water at room temperature (near 3350 cm^{-1}).[60] In interfacial and bulk environments, absorption in this region is primarily attributed to tetrahedrally coordinated water molecules with a distribution of hydrogen bonding interactions.[23,61,62]

The majority of the bulk-water IR spectrum in the hydrogen-stretch region is well fit by Gaussian distributions centered near 3200 and 3400 cm^{-1} and these components are often attributed to more ordered and disordered hydrogen-bonding configurations, respectively.[60] Those assignments would suggest that the increased photodissociation intensities observed at higher frequencies in the bonded-OH region is attributable to a hydrogen bond network around divalent calcium that is more distorted relative to bulk water. However, recent studies indicate that water molecules in bulk solution actually adopt a continuum of hydrogen bonding configurations, rather than discrete states,[61,62] and that increased absorbance cross sections at higher frequencies in the bonded-OH region may also be attributable to effects of the ionic charge on the infrared transition dipoles and the electric field of individual OH bonds.[61−63] The increased internal energy deposition of higher energy photons should also increase the photodissociation efficiency at higher frequencies slightly.

Spectral Changes with Increasing *n*. IRMPD spectra of $Ca^{2+}(H_2O)_n$, $n = 40$, 50, 61, and 69, were obtained under conditions expected to yield directly comparable intensities (Figure 5). Relative to the spectra obtained for smaller *n*, the differences between the spectra for these largest ions are more subtle (Figure 2). The free-OH region still exhibits sharp bands that are attributable to surface-bound water molecules. This suggests that the surfaces of these clusters are quite homogeneous. Bands *b* and *c* correspond respectively to the dangling-OH stretch of **AAD** and **AD** water molecules (Figure 3) and occur near 3685 and 3705 cm^{-1}. These frequencies are slightly red-shifted from those previously assigned for large $H^+(H_2O)_n$

(57) Weber, J. M.; Kelley, J. A.; Nielsen, S. B.; Ayotte, P.; Johnson, M. A. *Science* **2000**, *287*, 2461–2463.
(58) Ayotte, P.; Weddle, G. H.; Kim, J.; Johnson, M. A. *J. Am. Chem. Soc.* **1998**, *120*, 12361–12362.
(59) Sovago, M.; Campen, R. K.; Wurpel, G. W. H.; Muller, M.; Bakker, H. J.; Bonn, M. *Phys. Rev. Lett.* **2008**, *100*, 173901.
(60) Liu, D. F.; Ma, G.; Levering, L. M.; Allen, H. C. *J. Phys. Chem. B* **2004**, *108*, 2252–2260.
(61) Smith, J. D.; Saykally, R. J.; Geissler, P. L. *J. Am. Chem. Soc.* **2007**, *129*, 13847–13856.
(62) Smith, J. D.; Cappa, C. D.; Wilson, K. R.; Cohen, R. C.; Geissler, P. L.; Saykally, R. J. *Proc. Natl. Acad. Sci. U.S.A.* **2005**, *102*, 14171–14174.
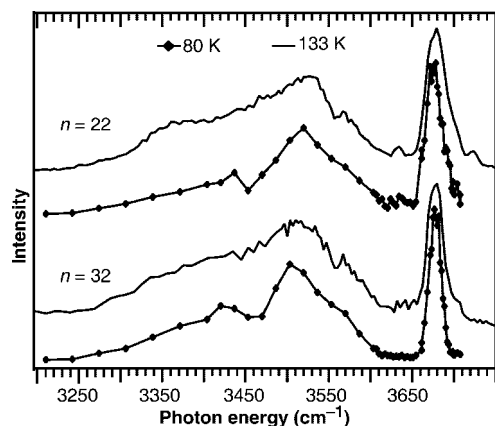(63) Corcelli, S. A.; Skinner, J. L. *J. Phys. Chem. A* **2005**, *109*, 6154–6165.

Figure 6. Photodissociation spectra of $Ca^{2+}(H_2O)_{22,32}$ obtained with copper jacket temperatures of 80 and 130 K.

(for $n \approx 20$, bands b and c occur near 3700 and 3720 cm^{-1}, respectively).[18,19,27] These bands for $Ca^{2+}(H_2O)_n$ continue to blue-shift slightly with increasing n, suggesting that the inductive effects of the divalent metal ion persist for many solvent shells. The intensity of band c is essentially constant for $n = 40$, 50, 61, and 69, but that of band b increases with n, which indicates the extent of hydrogen bonding on the cluster surface increases with cluster size.

Excluding the asymmetric stretches of double-donor water molecules near 3560 cm^{-1}, distinct bonded-OH bands are no longer resolved in these experiments by $n \approx 30$. This may be attributable to increasing congestion, broadening, and/or oscillator coupling with increasing cluster size. However, it is clear that the integrated areas of the bonded-OH regions of the spectra increase at much greater rates than those of the corresponding free-OH regions. Bands in bonded-OH region are primary attributable to the hydrogen stretches of interior water molecules, as well as smaller contributions from surface-bound water molecules that donate hydrogen bonds. This indicates that the "bulk" of these clusters grows at greater rates than the surface, consistent with the growth of a sphere.

Effects of Copper Jacket Temperature. Spectra of Ca^{2+}-$(H_2O)_{22}$ and $Ca^{2+}(H_2O)_{32}$ obtained at copper jacket temperatures of 80 and 130 K are shown in Figure 6. The spectra acquired at the colder copper jacket temperature exhibit significantly narrower peaks in the free-OH region. The peaks at 3680 cm^{-1} in the spectra of $Ca^{2+}(H_2O)_{22}$ have widths of ~23 and ~32 cm^{-1} fwhm with copper jacket temperatures of 80 and 130 K, respectively, whereas those for $Ca^{2+}(H_2O)_{32}$ have widths ~18 and ~24 cm^{-1} fwhm at those respective temperatures. In addition, the spectra acquired at the colder copper jacket temperature exhibit significantly less relative photodissociation in the bonded-OH region. The integrated photodissociation intensity in the bonded-OH regions (2900 − 3630 cm^{-1}) of $Ca^{2+}(H_2O)_{22}$ and $Ca^{2+}(H_2O)_{32}$ are 3 and 5 times greater than that in the corresponding free-OH regions (3630 − 3707 cm^{-1}) at the colder temperature, respectively, whereas those ratios at the warmer temperature are 5 and 7, respectively. Therefore, relative photodissociation in the bonded-OH regions of the spectra acquired at the colder temperature are roughly 30% less than those acquired at the warmer temperature.

At a copper jacket temperature of 130 K, the BIRD rates for the loss of one water molecule from $Ca^{2+}(H_2O)_{22}$ and $Ca^{2+}(H_2O)_{32}$ are 0.27 and 0.43 s^{-1}, respectively, whereas those rates are both <0.01 s^{-1} at 80 K. This indicates that the ions

trapped at the lower copper jacket temperature have significantly lower internal energies. The observed spectral differences may be attributable to increased populations of more enthalpically favored hydrogen bonding configurations at the lower copper jacket temperature. Alternatively, the fraction of the ion population that dissociates upon the absorption of a single laser photon is significantly smaller in the experiments performed at the colder copper jacket temperature. Absorption of multiple photons, the rate of which may not be directly proportional to the absorbance cross sections, plays a greater role at the colder copper jacket temperature and the spectral differences at the two temperatures may be a result of this nonlinearity. Additional experiments probing the spectra of these ions as a function of temperature are ongoing.

Hydrated Ion Clathrates. $H^+(H_2O)_{21}$[18,19,27] and NH_4^+-$(H_2O)_{20}$[64] appear as "magic numbers" in many mass spectra and the IRMPD spectra of these ions each predominantly exhibit a single free-OH band that is attributed to the dangling-OH stretch of **AAD** water molecules, whereas those of smaller clusters exhibit an additional free-OH band that is attributed to the dangling-OH stretch of **AD** water molecules. These results support assignment of these ions to icosahedral-like clathrate structures in which the excess charge is localized at the ion surface[18,19,27,64] and have generated considerable interest in identifying additional ionic clathrates.

Although the abundance of specific $Ca^{2+}(H_2O)_n$ ions can be maximized by varying source conditions,[48] no n values exhibit particularly enhanced abundance under a wide range of experimental conditions. The IRMPD spectra for all $n > 12$ exhibit photodissociation attributable to both **AD** and **AAD** water molecules. These results suggest that icosahedral-like clathrates are not formed for $Ca^{2+}(H_2O)_n$. Similar results were also reported for $Ni^+(H_2O)_n$ formed by laser vaporization.[7] One difference between $x(H_2O)_n$, $x = H_3O^+$ and NH_4^+, and these hydrated metal cations is that the excess charge is localized on the surface of the former and in the interior of the later. Additionally, H_3O^+ and NH_4^+ are tetrahedral like, whereas the latter are not. These results suggest that direct interactions between these metal ions and their first solvent shells affect the remaining hydrogen bond network and destabilize icosahedral-like structures. Therefore, it is likely that gas-phase clathrates will only be observed for hydrated clusters of ions with high propensities for the air/water interface or with tetrahedral coordination.[65,66] Additionally, these results suggests that even though the cavities of clathrate structures may be effective for trapping small neutral molecules,[67] the cavities may not be effective for trapping metal ions.

Conclusions

Results from infrared action spectroscopy provide interesting new insights into the solvation of divalent calcium. The coordination number of divalent calcium is eight when solvated by 12 water molecules, consistent with many bulk-solution studies,[32] whereas previous results for smaller hydrated divalent ions are most consistent with a coordination number of six. Spectral changes with increasing cluster size, particularly those

(64) Diken, E. G.; Hammer, N. I.; Johnson, M. A.; Christie, R. A.; Jordan, K. D. *J. Chem. Phys.* **2005**, *123*, 164309.
(65) Petersen, P. B.; Saykally, R. J. *Annu. Rev. Phys. Chem.* **2006**, *57*, 333–364.
(66) Pegram, L. M.; Record, M. T. *Proc. Natl. Acad. Sci. U.S.A.* **2006**, *103*, 14278–14281.
(67) Koh, C. A. *Chem. Soc. Rev.* **2002**, *31*, 157–167.

in the free-OH region, provide detailed information on the hydrogen-bonding motifs present in these ions. Spectral features for the largest ions, which have effective concentrations of divalent calcium that are less than 1 M and are the largest isolated hydrated cluster ions yet probed using vibrational spectroscopy, exhibit only subtle differences.

All IRMPD spectra exhibit intense free-OH bands, even at very large cluster sizes, and share many similarities with the sum-frequency spectra of the air/water interface.[23,60,68] These spectra hint at the potential of using large hydrated clusters to obtain detailed information on the structure and dynamics of interfacial environments. For example, specific cluster ions of interest can be isolated, enabling fine control of counterions and solvent, and eliminating interfering surfactant contaminates.

Additionally, cluster sizes can be varied, enabling clearly defined probe depths for interfacial regions of interest.

Supporting Information Available: Full citation for ref 51. This material is available free of charge via the Internet at http://pubs.acs.org.

JA804621R

(68) Du, Q.; Superfine, R.; Freysz, E.; Shen, Y. R. *Phys. Rev. Lett.* **1993**, *70*, 2313–2316.